ELSEVIER

Materials Science and Engineering A 481–482 (2008) 414–419

MATERIALS SCIENCE & ENGINEERING A

www.elsevier.com/locate/msea

Hard X-ray studies of stress-induced phase transformations of superelastic NiTi shape memory alloys under uniaxial load

M. Hasan [a,b], W.W. Schmahl [a,*], K. Hackl [c], R. Heinen [c], J. Frenzel [d], S. Gollerthan [d], G. Eggeler [d], M. Wagner [d], J. Khalil-Allafi [e], A. Baruj [f]

[a] *Ludwig-Maximilian Universität, Department für Geo- und Umweltwissenschaften, Sektion Kristallographie, Theresienstraße 41, 80333 München, Germany*

[b] *Ruhr-Universität Bochum, Fakultät für Geowissenschaften, Universitätsstraße 150, 44780 Bochum, Germany*

[c] *Ruhr-Universität Bochum, Institut für Mechanik, Lehrstuhl für Allgemeine Mechanik, Universitätsstraße 150, 44780 Bochum, Germany*

[d] *Ruhr-Universität Bochum, Institut für Werkstoffe, Universitätsstraße 150, 44801 Bochum, Germany*

[e] *Sahand University of Technology, Faculty of Materials Engineering, Tabriz, Iran*

[f] *Instituto Balseiro Centro Atomico Bariloche, 8400 S.C. de Bariloche, Argentina*

Received 17 May 2006; received in revised form 6 February 2007; accepted 22 February 2007

Abstract

We examined the texture evolution in a superelastic $Ni_{50.7}Ti_{49.3}$ (numbers indicate at.%) alloy under applied uniaxial stress using high-energy synchrotron X-ray diffraction in transmission geometry. Texture information is identified from the intensity variations along Debye–Scherrer rings recorded on area detector diffraction images. The $1\,1\,0_A$ austenite plane normals are aligned in the rolling direction and $2\,0\,0_A$ is in the transverse direction. Due to the B2–B19′ lattice correspondence, the $1\,1\,0_A$ peak splits into four martensite peaks $0\,2\,0_M$, $\bar{1}\,1\,1_M$, $0\,0\,2_M$ and $1\,1\,1_M$. The stress-induced martensite is strongly textured from twin variant selection in the stress field with $0\,2\,0_M$ aligned in the loading direction while the maxima corresponding to $\bar{1}\,1\,1_M$, $0\,0\,2_M$ and $1\,1\,1_M$ are at 60°, 67° and 75° from the loading direction. (B19′ unit cell setting: $a = 2.87$ Å, $b = 4.59$ Å, $c = 4.1$ Å, $\gamma = 96.2°$). A comparison between the experimental and recalculated distribution densities for the polycrystalline NiTi shows a reasonable agreement. In addition, we compare our experimental results with a micromechanical model which is based on total energy minimization. In this case, we also observe an overall agreement.

Keywords: Twin variant texture; Superelasticity; Stress-induced martensite; Cold rolled B2 austenite; NiTi

1. Introduction

The shape memory and the superelasticity of NiTi alloys are related to the martensitic phase transformation from the cubic B2 austenite (space group *Pm*3*m*) to the monoclinic B19′ (space group $P2_1/m$) martensite phase [1]. The phase transformation can be induced by stress as well as by changes in temperature. The recoverable strain is related to the ability of the material to produce a compliant alignment of the martensite twin variants in the stress field. In other words, the crystallographic texture of martensite twin variants determines the recoverable strain and other performance parameters [2]. However, there are not many reports [2,3] of stress-induced martensite texture measurements using hard X-rays on superelastic NiTi tensile specimens upon uniaxial loading. Shaw and Kyriakides [4–6] demonstrated that the deformation causing the superelastic plateau in the stress–strain curve of flat tensile-test specimens is localized in Lüders-band-like transformation shear bands (TSB). The phase contents and lattice strains in the TSB have been imaged by synchrotron diffraction experiments [7]. The uniaxial stress field favours the growth of particular martensite variants over others. A thermodynamic model for polycrystalline shape memory alloys (SMAs) considering the orientation distribution of the various martensite-variants as internal variables has been developed [8] in order to describe the material behaviour. The mathematical and numerical aspects of this model can be found elsewhere in this volume [9]. The experimental results obtained in the present paper are used in [9].

* Corresponding author. Tel.: +49 89 2180 4311; fax: +49 89 2180 4334.
E-mail address: wolfgang.schmahl@lrz.uni-muenchen.de (W.W. Schmahl).

0921-5093/$ – see front matter © 2007 Published by Elsevier B.V.
doi:10.1016/j.msea.2007.02.156

2. Experiments

In the present study a tensile test sample of 1.8 mm thickness, 6 mm width, and 10 mm gauge length was produced from a Ni-rich binary polycrystalline NiTi alloy with a nominal content of 50.7 at.%Ni, purchased from Memory Metalle GmbH, Weil am Rhein, Germany. The material was solution annealed at 850 °C for 15 min and quenched in water. It was subsequently cold rolled with 10% thickness reduction at −150 °C. Finally, it was aged at 500 °C for 6 min in order to reduce the dislocation density. Accurate tensile testing was done in the laboratory using a Schenk Model PC 160 servo-hydraulic tensile testing instrument. In situ diffraction experiments with hard X-rays were carried out at the wiggler-beamlime BW5 of the Hamburg Synchrotron Laboratory (HASYLAB), DESY, Germany. The beam size was 250 μm × 250 μm. A wavelength of 0.137443(9) Å was selected to obtain satisfactory diffractograms in transmission geometry on the MAR 2300 image plate detector placed at 900 mm from the sample. An extensometer was not fitted on the sample in order to avoid X-ray diffraction (XRD) peaks not coming from the sample. The geometry of the stress frame allowed transmission in one direction only such that the circle containing the tensile axis and the transverse direction were covered.

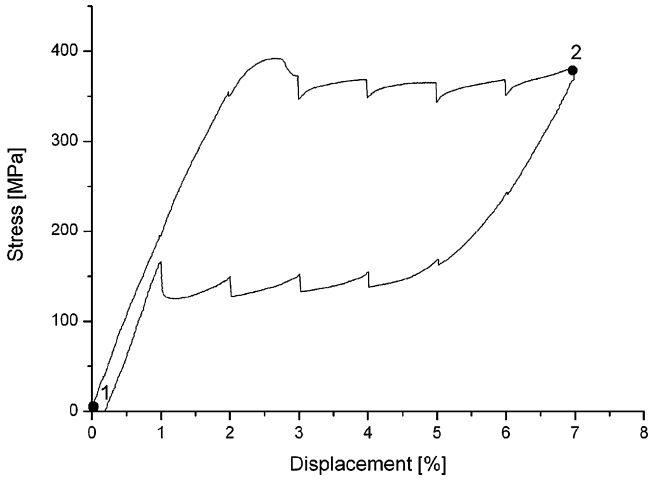

Fig. 1. Crosshead-displacement vs. stress curves of the Ni-rich $Ni_{50.7}Ti_{49.3}$ alloy as measured in the in situ diffraction experiment. The solid points numbered 1 and 2 describe the data analysed in this paper.

3. Data analysis

The data processing typically requires several steps for quantitative texture analysis of polycrystalline materials. Using the software FIT2D [10] the image plate data were corrected for centre and tilt misalignments. Local background subtraction and polarization correction is also applied to the measured intensities [11]. Diffraction intensities were extracted with FIT2D into a multicolumn ASCII spread sheet [12], where each column corresponds to an intensity distribution along the azimuth for a particular 2θ value. The peak positions were identified from full profile analysis using the GSAS refinement code [13] and intensity versus azimuth data for particular reflections were extracted. It needs to be considered that the diffraction ring is not circular if the material is under stress [14]. Although we get incomplete pole figures from the Debye–Scherrer rings in a single two-dimensional diffraction image, it is possible to construct an orientation distribution function (ODF) for the B2 and the B19′ phase from the combined information using several rings. To obtain the ODF with the method described by Wenk and Grigull [14] we used the WIMV [15] algorithm of the BEARTEX [16] code with the $1\,1\,0_A$, $2\,0\,0_A$, $2\,2\,0_A$, and $2\,2\,2_A$ Debye–Scherrer rings of austenite, and the $0\,2\,0_M$, $0\,1\,1_M$, $1\,0\,0_M$, $\bar{1}\,1\,0_M$, $1\,0\,1_M$, $1\,1\,0_M$, $\bar{1}\,1\,1_M$, $0\,0\,2_M$, and $1\,1\,1_M$ rings of B19′ martensite. Recalculated pole figures were then obtained

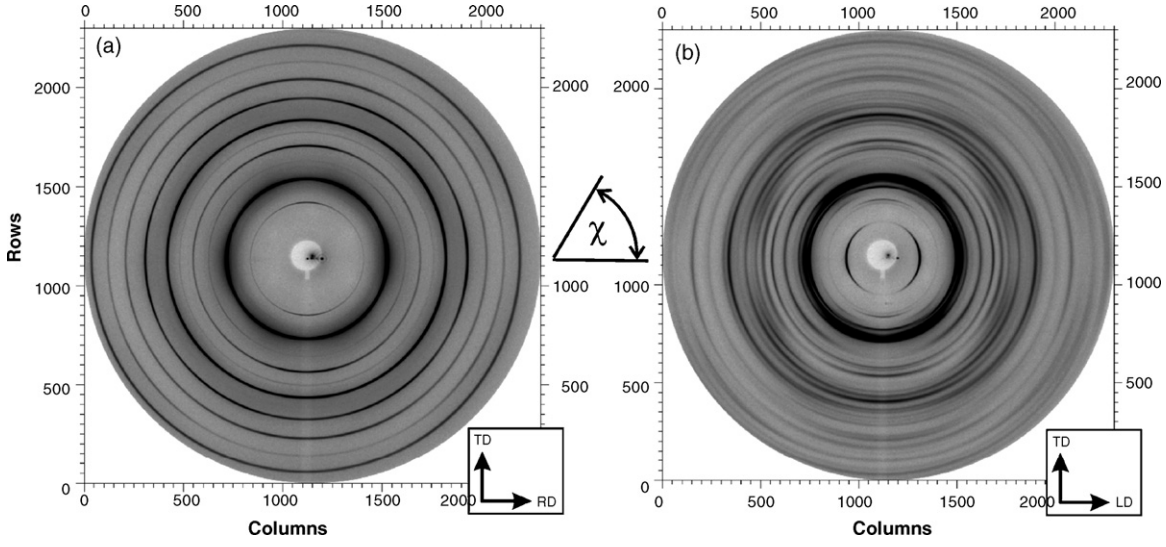

Fig. 2. Image plate recordings of the diffractograms of the original B2 austenite in the unstressed state (left, a) and the transformed state (right, b) corresponding to point 2 of Fig. 1. The rolling direction (RD), loading direction (LD), and transverse directions (TD) are indicated as well as the azimuth angle χ. The loading is parallel to the original rolling direction. The material in the unstressed state (left, a) shows a moderate rolling texture. The strong texture due to twin variant selection in the stress-induced martensite can be seen from the pronounced intensity variations along the Debye-Scherrer rings in the diffractogram on the right.

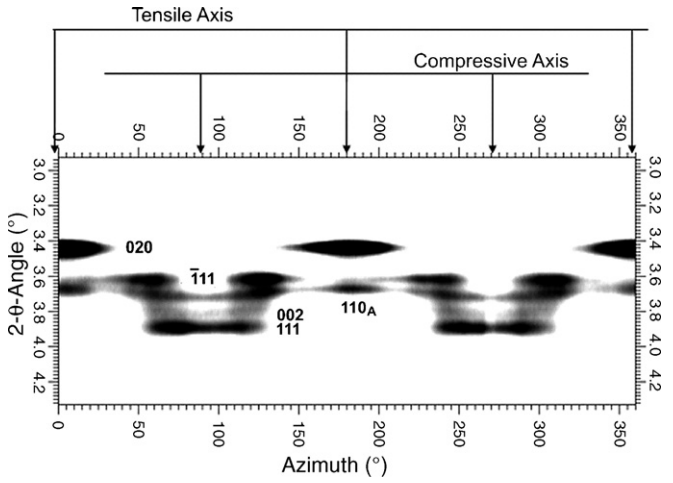

Fig. 3. Display of the intensity distribution of the strongest Debye–Scherrer rings in the diffractogram of point 2 in Fig. 1 as a function of azimuth angle χ (refer to Fig. 2). The azimuth of 0° and 180° corresponds to the tensile direction, 90° and 270° mark the transverse direction. The 1 1 0 diffraction line of austenite is labelled as $1\,1\,0_A$, the intensities for the monoclinic phase are labelled without subscript.

for the observed directions from the ODF. In BEARTEX, pole figures are divided into 5° × 5° pole distance/azimuth cells.

4. Results and discussion

The stress versus nominal strain curve obtained during the diffraction experiment is shown in Fig. 1. The points in Fig. 1 indicate where the diffractograms were taken. The kinks in the plateau of the stress-strain curve are related to a relaxation of the state of the sample occurring during the X-ray exposure and data readout-time [17]. For a textured NiTi sheet produced by cold rolling, loading along the rolling direction results in a flat stress plateau in the stress-strain curve which can also be observed in Fig. 1. Fig. 2 shows the obtained characteristic diffractograms for austenite (Fig. 2a) and the transformed state (Fig. 2b). The direction of tensile stress is horizontal in Fig. 2, and the vertical scattering direction is the direction of transverse contraction. The prominent $1\,1\,0_A$ peak splits into four martensite peaks, $0\,2\,0_M$, $\bar{1}\,1\,1_M$, $0\,0\,2_M$ and $1\,1\,1_M$ which show intense stress-induced texturing as shown in Fig. 3 (B19′ unit cell setting used for indexing: $a = 2.87$ Å, $b = 4.59$ Å, $c = 4.1$ Å, $\gamma = 96.2°$). It can be seen from Fig. 3 that the austenite remains present throughout the plateau of the stress–strain curve. The stress-induced martensite renders the interpretation of the diffractogram more complicated due to overlapping peaks that are visible in Fig. 3. To take all peaks properly into account, we employed a full profile Rietveld refinement using a spherical harmonics texture model. At the end of the plateau (point 2 in Fig. 1), 10 wt.% residual austenite is estimated from the Rietveld refinement which corresponds well to our previous estimates [7]. It is interesting to observe in Fig. 3 that the residual austenite $1\,1\,0_A$ line is slightly sinusoidal as the austenite is under stress. As the austenite grains are inclusions in the martensite matrix, the yielding of the matrix by transformation transfers load on the residual austenite [18].

The stress-free austenite shows a rolling texture, where the $1\,1\,0_A$ are preferentially oriented in the rolling direction (which is also the axis of tensile stress in the experiment), while $2\,0\,0_A$ are preferentially oriented along the transverse direction, and $2\,2\,2_A$ are preferentially oriented at an angle of 35° from the rolling direction. The obtained ODF reproduces the features of the experimental pole density distribution (Fig. 4). Complete recalculated pole figures displaying also the ODF-modelled unobserved regions of the pole figure are displayed in Fig. 5. As the experimental pole figure information is limited to the

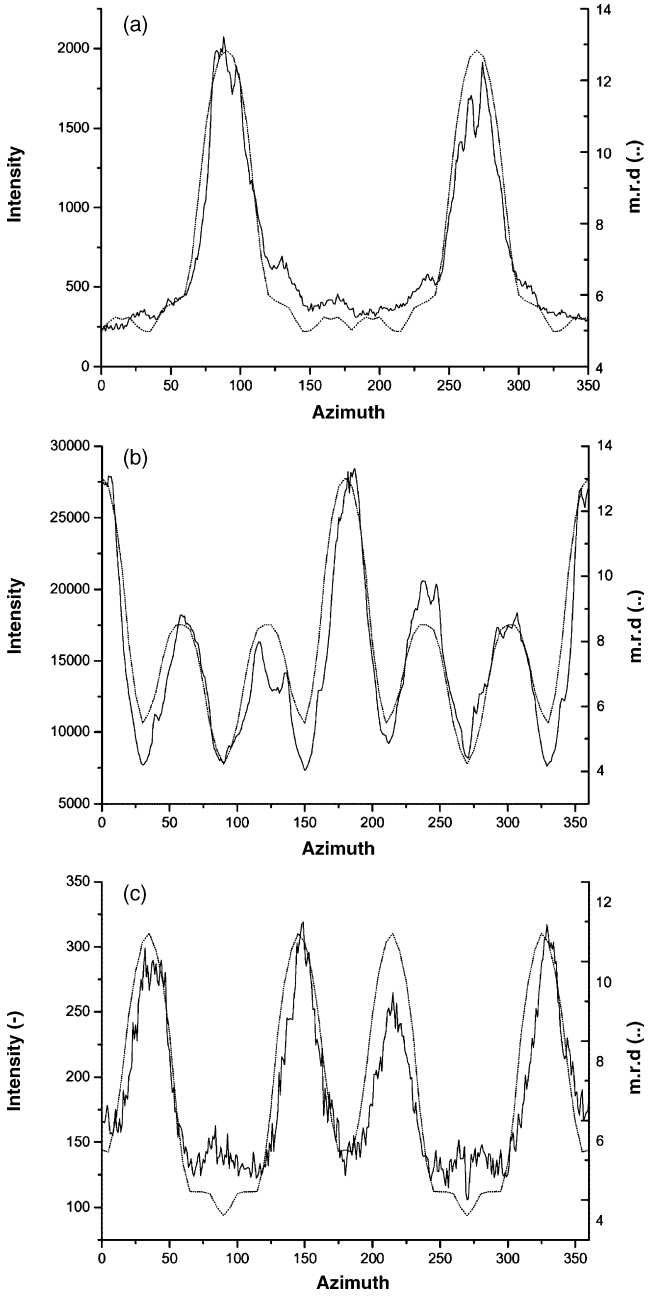

Fig. 4. Intensity distribution of the original B2 austenite along the azimuth of (a) $2\,0\,0_A$, (b) $1\,1\,0_A$, (c) $2\,2\,2_A$ diffraction rings in the stress-free state. The rolling direction corresponds to azimuths of 0° and 180°. The left- side axis shows the observed intensity whereas the right-side axis shows the recalculated pole density. The apparent data scatter is a result of the graininess of the sample.

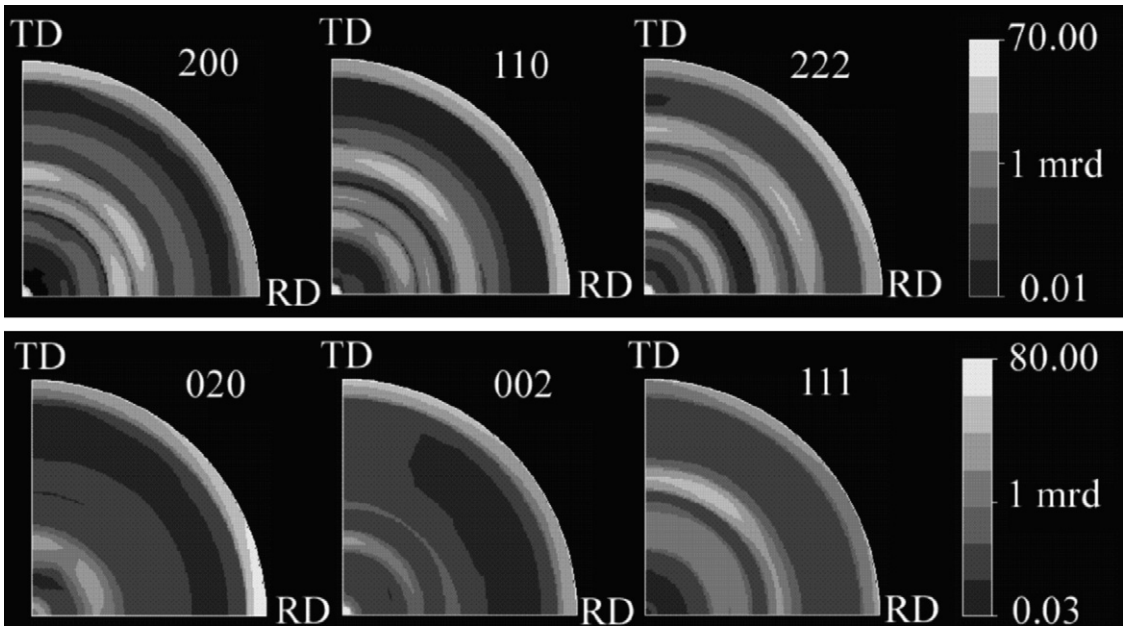

Fig. 5. Selected recalculated pole figures. Top: unstressed B2 austenite $2\,0\,0_A$, $1\,1\,0_A$, and $2\,2\,2_A$. Bottom: stress-induced martensite $0\,2\,0_M$, $0\,0\,2_M$, and $1\,1\,1_M$. All plots are stereographic projections; only one quadrant is shown as the assumed sample symmetry is mmm; logarithmic density scales (normalized to m.r.d.). Rolling (RD) from left to right, transverse directions (TD) from top to bottom. Note that the experimental technique allowed observation only of the outer ring of the pole figures. The inner part is an estimate based on the incomplete information from all used reflections.

outer circle of these stereograms, the inner part is an estimate from the observed incomplete pole figures of the reflections used and it must be treated with caution. Although we needed to use the obtained full ODF of the cold-rolled austenite as a basis distribution function for the application of the thermodynamic model of martensite formation in the stress field [9], we can draw conclusions only from the actually observed data.

For the martensite diffraction rings $0\,2\,0_M$, $0\,0\,2_M$ and $1\,1\,1_M$ numerical intensities as a function of azimuth in section of constant 2θ are shown in Fig. 6. According to the experimental observation displayed in Fig. 6(a)–(c) (solid curves), the $0\,2\,0_M$ poles show a pronounced maximum in pole density in the direction of tensile stress, i.e. at 0° and 180° azimuth. The pole density maxima for $\bar{1}\,1\,1_M$, $0\,0\,2_M$, and $1\,1\,1_M$ are at 60°, 67°, and 75° away from the 0° and 180° azimuths. Minimum pole densities for $0\,2\,0_M$ are found in the transverse direction at 90° and 270°, and for $\bar{1}\,1\,1_M$, $0\,0\,2_M$ and $1\,1\,1_M$ there is very little pole density found in the direction of tensile stress. Recalculated pole figures from the martensite ODF data are shown for the observed directions in Fig. 7 (estimated complete pole figures are displayed in Fig. 5). A comparison of Figs. 6 and 7 shows that the recalculated partial pole figures show a reasonable agreement with the original experimental data and even more with the pole densities obtained with the micromechanical model.

5. Summary

Texture information on the twin-variant alignment in stress-induced martensite forming in a polycrystalline superelastic NiTi specimen under uniaxial stress was extracted from single-orientation 2D diffraction images in transmission geometry. The diffraction rings of the high-energy X-rays simultaneously cover the tensile axis and the transverse axis as well as the circle of orientations between these principal axes (while information in the normal direction can not be accessed with the present set-up). A thermodynamic micromechanical model based on total energy minimization of the twin variant configuration for a polycrystalline material in a stress field is described elsewhere in this issue [9]. The model calculation shows a reasonable agreement with our experimental data. The results can be rationalized from the fact that the $0\,2\,0_M$ spacing shows the largest expansive transformation strain for the set of twelve martensite lattice planes corresponding to the twelve $1\,1\,0$ type planes of austenite; thus $0\,2\,0_M$ preferentially aligns with the axis of tensile stress when the stress-induced martensite is formed. Because the original material shows a rolling texture and preferred orientation of $1\,1\,0_A$ along the tensile axis, the alignment of $0\,2\,0_M$ in the tensile axis is easy for many grains, and thus the $0\,2\,0_M$ pole density maximum becomes particularly pronounced and the specimen can provide a large recoverable pseudelastic tensile strain in the rolling direction. The cubic symmetry of austenite places other $1\,1\,0_A$ pole density maxima at 60° azimuthal angles with respect to the rolling direction and the direction of tensile stress. Correspondingly, the $\bar{1}\,1\,1_M$, $0\,0\,2_M$, and $1\,1\,1_M$ poles align near these azimuths, with a small deviation from 60° due to the monoclinic distortion of the martensite phase.

Acknowledgement

This work was funded by the Helmholtz Gemeinschaft under VH-VI-102 and SFB 459 of the Deutsche Forschungsgemeinschaft.

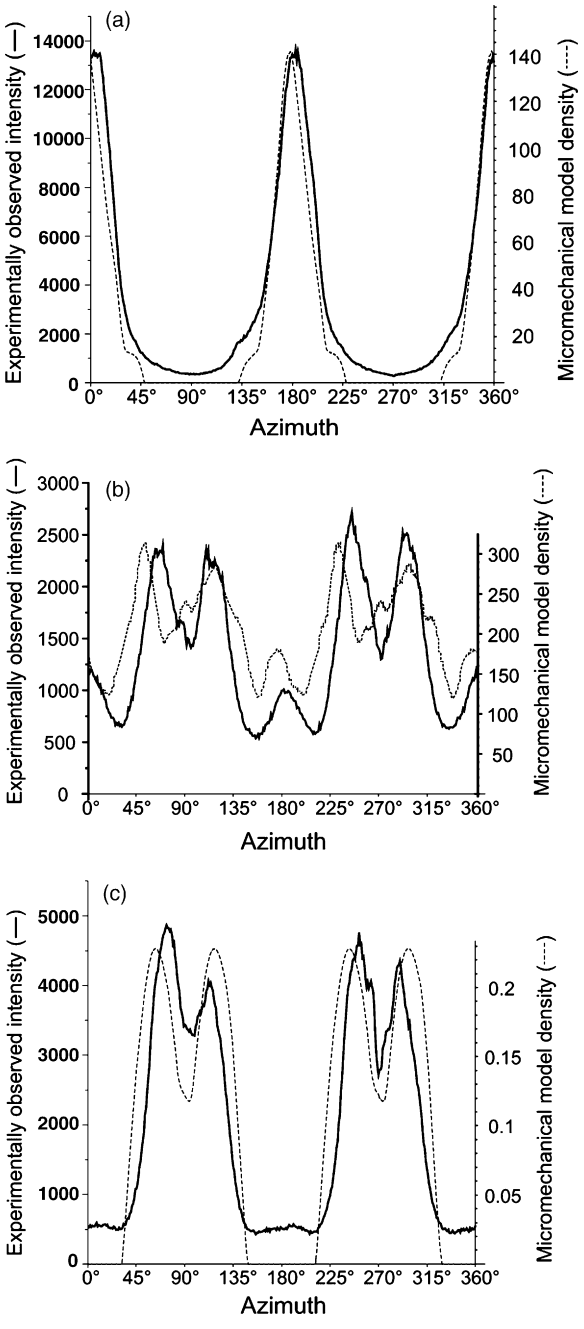

Fig. 6. Intensity distribution along the azimuth of (a) $0\,2\,0_M$, (b) $0\,0\,2_M$, (c) $1\,1\,1_M$ diffraction rings in the martensite phase obtained from Fig. 3. The solid curve has been obtained from experiments and the dotted curve has been obtained from the micromechanical model. The left-side axis shows the experimentally obtained intensity whereas the right-side axis shows the micromechanical model density (arbitrary scale). The loading direction corresponds to azimuths of 0° and 180°.

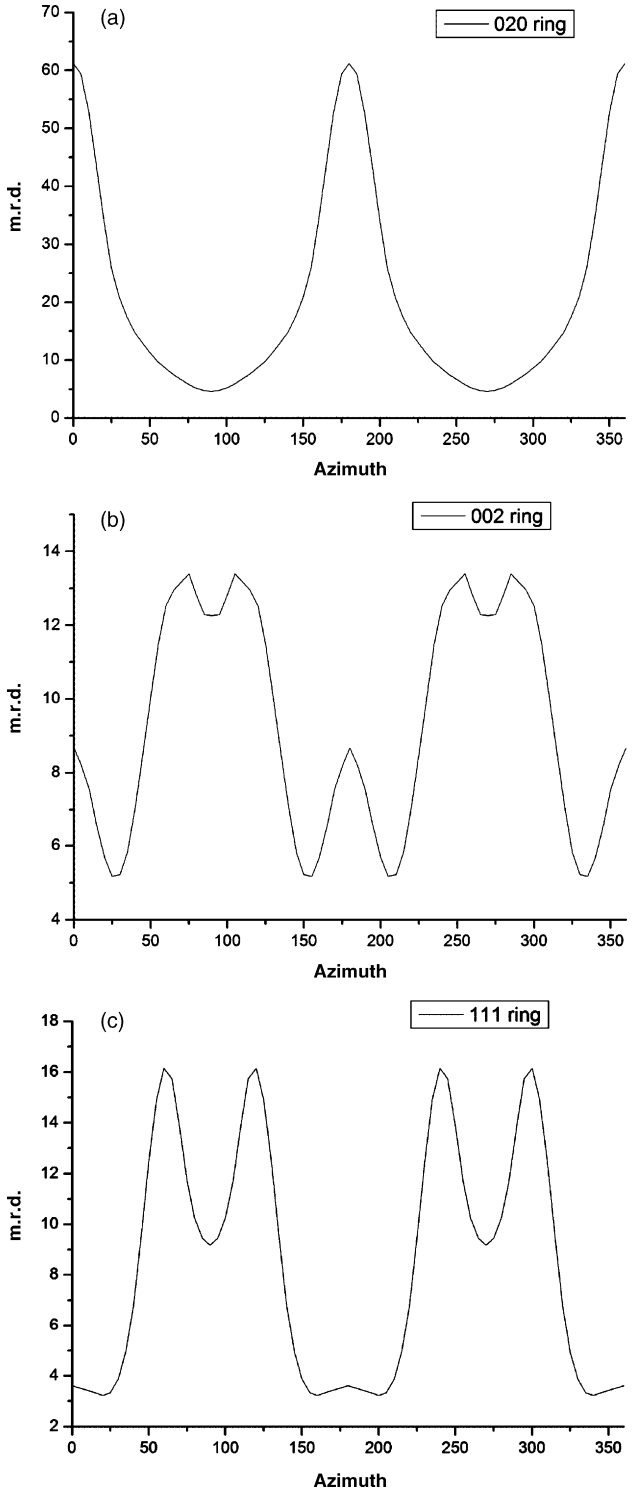

Fig. 7. Recalculated numerical density distribution along the azimuth of (a) $0\,2\,0_M$, (b) $0\,0\,2_M$, (c) $1\,1\,1_M$ diffraction rings in the martensite phase.

References

[1] K. Otsuka, C.M. Wayman (Eds.), Shape Memory Materials, Cambridge University Press, Cambridge, UK, 1998.
[2] J.H. Mulder, P.E. Thoma, J. Beyer, Z. Metallkd. 84 (1993) 501–508.
[3] Q.S. Zheng, Y. Liu, Philo. Maga. A 82 (2002) 665–683.
[4] J.A. Shaw, S. Kyriakides, J. Mech. Phys. Solids 43 (1995) 1243–1281.
[5] J.A. Shaw, S. Kyriakides, Int. J. Plast. 13 (1997) 837–871.
[6] J.A. Shaw, S. Kyriakides, Acta Mater. 45 (1997) 683–700.
[7] W.W. Schmahl, J. Khalil-Allafi, B. Hasse, M. Wagner, A. Heckmann, Ch. Somsen, Mater. Sci. Eng. A 378 (2004) 81–85.
[8] K. Hackl, M. Schmidt-Baldassari, W. Zhang, Mater. Sci. Eng. A 378 (2004) 503–506.
[9] K. Hackl, R. Heinen, W.W. Schmahl, M. Hasan, (this issue): Experimental Verification of a Micromechanical Model for Polycrystalline Shape Memory Alloys in Depence of Martensite Orientation Distributions.

[10] A.P. Hammersley, S.O. Svensson, A. Thompson, H. Graafsma, A. Kvick, J.-P. Moy, Rev. Sci. Instrum. 66 (1995) 2729–2733.
[11] F. Heidelbach, C. Riekel, H.-R. Wenk, J. Appl. Cryst. 32 (1999) 841–849.
[12] S. Merkel, H.-R. Wenk, J. Shu, G. Shen, P. Gillet, H.-K. Mao, R.J. Hemley, J. Geophys. Res. 107 (2002) 2271–2288.
[13] R.B. von Dreele, J. Appl. Cryst. 30 (1997) 517–525.
[14] H.-R. Wenk, S. Grigull, J. Appl. Cryst. 36 (2003) 1040–1049.
[15] S. Matthies, G.W. Vinel, Phys. Status Solidi B 112 (1982) K111–K114.
[16] H.R. Wenk, S. Matthies, J. Donovan, D. Chateigner, J. Appl. Cryst. 31 (1998) 262–269.
[17] L.C. Brinson, I. Schmidt, R. Lammering, J. Mech. Phys. Solids 52 (2004) 1549–1571.
[18] G. Tan, Y. Liu, P. Sittner, M. Saunders, Scripta Mater. 50 (2004) 193–198.